Hydroxybenzo[b]quinolizinium Ions: Water-Soluble and Solvatochromic Photoacids

Katy Schäfer, Heiko Ihmels, Cornelia Bohne, Karolina Papera Valente, and Anton Granzhan

October 2016

This article was originally published at:

http://dx.doi.org/10.1021/acs.joc.6b01991

Schafer, K. et al., (2016). Hydroxybenzo[b]quinolizinium Ions: Water-Soluble and Solvatochromic Photoacids. *The Journal of Organic Chemistry*, 81, 10942-10954. doi: 10.1021/acs.joc.6b0199

JOC The Journal of Organic Chemistry

Article

pubs.acs.org/joc

Hydroxybenzo[*b*]quinolizinium Ions: Water-Soluble and Solvatochromic Photoacids

Katy Schäfer,[†] Heiko Ihmels,*[,†] Cornelia Bohne,[‡] Karolina Papera Valente,[‡] and Anton Granzhan[§]

[†]Department of Chemistry - Biology and Center of Micro and Nanochemistry and Engineering, University of Siegen, Adolf-Reichwein-Strasse 2, D-57068 Siegen, Germany

[‡]Department of Chemistry, University of Victoria, PO Box 1700 STN CSC, Victoria, BC Canada V8W 2Y2

[§]Institut Curie, PSL Research University and Université Paris Sud, Université Paris-Saclay, CNRS UMR9187, INSERM U1196, F-91405 Orsay, France

Supporting Information

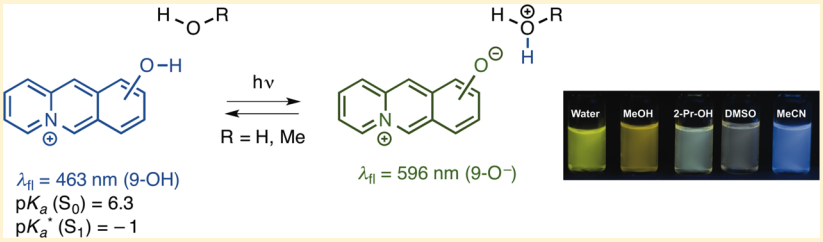

ABSTRACT: It is shown by photometric and fluorimetric analysis, along with supporting theoretical calculations, that hydroxy-substituted benzo[*b*]quinolizinium derivatives display the characteristic features of organic photoacids. Specifically, the experimental and theoretical results confirm the strong acidity of these compounds in the excited state ($pK_a^* < 0$). The combination of the prototropic properties of 8- and 9-hydroxybenzo[*b*]quinolizinium with the particular solvent−solute interactions of the excited acid and its conjugate base leads to a pronounced fluorosolvatochromism, hence the emission maxima shift from 468 nm (8-hydroxybenzo[*b*]quinolizinium) or 460 nm (9-hydroxybenzo[*b*]quinolizinium) in CH_3CN to 507 and 553 nm in DMF, respectively. This novel type of photoacid represents several features that may be used for applications as water-soluble fluorescent probes or as a source for the photoinduced supply of acidity.

INTRODUCTION

Acid−base equilibria constitute the foundation of numerous relevant processes in chemistry, biology, and physics. Specifically, several chemical reactions proceed at reasonable rate only upon acid or base catalysis.[1] Moreover, acid−base equilibria are important in biological systems, because the pH of the (micro)environment has a strong influence on the structure and biological activity of, for example, proteins and nucleic acids or drugs.[2] The adjustment of the pH of a solution or the initiation of an acid-catalyzed reaction is usually accomplished by the addition of an appropriate acid, which is available from a pool of substrates that may serve any desired requirement and may be modified according to the desired purpose.[3] Nevertheless, in many cases, local and temporal control of the proton concentration and activity is desirable, which may be realized by photoacids.[4] For example, photoacid generators such as triphenylsulfonium hexafluorophosphate derivates[5] decompose upon irradiation to yield HPF_6 as primary product. This photogenerated acid is employed, for example, for the processing of coatings, glues, photoresists, or micro- and nanostructuring of organic materials in micro-systems technology,[6] in the synthesis of oligonucleotides,[7] for the rapid release of protons in studies of membrane processes,[8] or in photodynamic therapy.[9] On the other hand, compounds that are only weakly acidic in the ground state but exhibit a high acidity in the excited state may be used as *reversible* photoacids.[10] In this context, hydroxy-substituted aromatic compounds figure as the paradigm of organic photoacids, and especially naphthol and hydroxypyrene derivatives serve as ideal model compounds and have been investigated in detail over recent decades.[10,11] Hence, 1- or 2-naphthol and electron-acceptor-substituted derivatives thereof are weak or moderate acids in the ground state, whereas their pK_a^*, that quantifies the acidity in the excited state, is lower by several orders of magnitude.[11] Compounds with a $pK_a^* < 0$, such as, for example, 5,8-dicyano-2-naphthol ($pK_a^* = -4.5$), are usually classified as superphotoacids. Complementary to hydrocarbon arenes, hydroxy-substituted hetarenes constitute a promising class of photoacids, specifically as they usually provide sufficient water solubility. In that context, quinoline and quinolinium derivatives were established as novel class of photoacids.[12,13] Along these lines, we discovered the 8-hydroxybenzo[*b*]-quinolizinium ion (**1b**) as a water-soluble, solvatochromic photoacid. In this derivative, the pyridinium unit serves as a strong intrinsic acceptor functionality that supports the

Received: August 13, 2016
Published: October 18, 2016

DOI: 10.1021/acs.joc.6b01991
J. Org. Chem. 2016, 81, 10942−10954

Scheme 1. Acid–base Equilibrium of Hydroxybenzo[*b*]quinolizinium (1b)

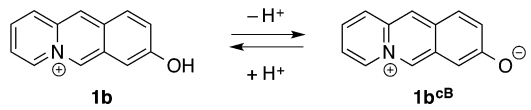

formation of the conjugate base **1b**^{cB} (Scheme 1).[14] Benzo[*b*]quinolizinium was chosen as elemental scaffold because, in contrast to most hydrophobic polyaromatic hydroxyarenes, benzo[*b*]quinolizinium is sufficiently water-soluble and enables studies and applications in aqueous media.[15] Moreover, the bridgehead nitrogen atom is not basic and does not perturb the acid–base reactions in the ground and excited state in a competing prototropic equilibrium. Our preliminary results showed that derivative **1b** exhibits promising photoacidic properties along with a pronounced fluorosolvatochromism, that is the result of the excited state deprotonation.[14] Therefore, we extended our studies to the four isomers **1a–d** (Chart 1), as well as to their methylated derivatives **2a–c** for comparison, to examine whether these properties are a general feature of hydroxybenzo[*b*]quinolizinium derivatives. Herein we present the photophysical studies of hydroxybenzo[*b*]quinolizinium isomers **1a–d** and demonstrate that these derivatives constitute a novel class of solvatochromic photoacids.

Chart 1. Structure and Numbering of Hydroxy- and Methoxy-Substituted Benzo[*b*]quinolizinium Derivatives 1a–d and 2a–d

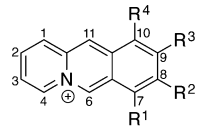

1a: R^1 = OH; R^2 = R^3 = R^4 = H
1b: R^2 = OH; R^1 = R^3 = R^4 = H
1c: R^3 = OH; R^1 = R^2 = R^4 = H
1d: R^4 = OH; R^1 = R^2 = R^3 = H
2a: R^1 = OMe; R^2 = R^3 = R^4 = H
2b: R^2 = OMe; R^1 = R^3 = R^4 = H
2c: R^3 = OMe; R^1 = R^2 = R^4 = H
2d: R^4 = OMe; R^1 = R^2 = R^3 = H

RESULTS

Synthesis. The benzo[*b*]quinolizinium derivatives **1a–d** and **2a–c** were synthesized by the cyclodehydration method[16] and identified by comparison with literature data.[17] Except for compounds **1a**, **2a**, and **1d**, the employed hydroxy- and methoxy-substituted benzo[*b*]quinolizinium derivatives were already known.[17] Both derivatives **1a** and **2a** were obtained starting from the reaction of 2-(bromomethyl)anisole **3a** with 2-(1,3-dioxolan-2-yl)pyridine to give the *N*-benzylpyridinium derivative **4a-Br** (Scheme 2). The product was obtained as the bromide salt and converted to tetrafluoroborate **4a-BF$_4$** by ion metathesis. Treatment of the latter with polyphosphoric acid (PPA) led to the formation of the 7-methoxybenzo[*b*]quinolizinium (**2a**) in 19% yield. The methyl ether was cleaved by the reaction with HBr (48%) to give 7-hydroxybenzo[*b*]quinolizinium (**1a**) in 41% yield. Analogous to this procedure, the isomeric 10-hydroxybenzo[*b*]quinolizinium (**1d**) was obtained in 31% yield by the reaction of the known 10-methoxybenzo[b]quinolizinium[17c] with HBr. Novel compounds **1a**, **2a**, and **1d** were identified and fully characterized by 1D- and 2D-NMR spectroscopy, mass spectrometry, and elemental analysis.

Solvatochromic Properties. Absorption and emission spectra of the hydroxybenzo[*b*]quinolizinium derivatives **1a–d** as well as those of the *O*-methylated derivatives **2a–d** were recorded in different solvents (Table 1). The absorption spectra of the hydroxybenzo[*b*]quinolizinium derivatives **1b** and **1c** display long-wavelength absorption maxima ranging from 357 nm (**1b**) and 385 nm (**1c**) in water to 428 nm (**1b**) and 414 nm (**1c**) in DMSO (Table 1, Figure 1, A2 and A3). In contrast, derivatives **1a** and **1d** cover a significantly smaller absorption range, i.e. from 407 nm in water to 424 nm in DMSO (**1a**) and from 377 nm in CH_3CN to 469 nm in DMSO (**1d**) (Table 1). In most cases, the maximum absorption is accompanied by a red-shifted broad shoulder at 480 and 550 nm (Figure 1, A1–4). The absorption spectra of methoxy-substituted derivatives **2a–d** are essentially the same in different solvents with absorption maxima between 371 and 415 nm (Table 1).

Derivative **1a** exhibits a fluorescence band with a maximum of 501 nm in water, that does not change significantly in different solvents (Figure 1, B1). In contrast, derivatives **1b–d** show a pronounced fluorosolvatochromic behavior (Figure 1, Table 1). For example, the emission maxima of **1b** and **1c** shift from 468 nm (**1b**) and 460 nm (**1c**) in CH_3CN to 507 nm (**1b**) and 553 nm (**1c**) in DMF. In some cases, a dual emission was observed (Figure 1, B2–4). For example, in DMSO, a second, less intense emission band is formed at 654 nm (**1b**) and 476 nm (**2c**) along with the maxima at 504 nm (**1b**) and 558 nm (**1c**). Furthermore, in the case of **1c**, dual emission was observed in methanol solution, whereas in other alcohols (1-PrOH, 1-BuOH, 1-pentanol, 1-hexanol) only the long-wavelength absorption band was observed (Supporting Information, Figure S9). In general, the emission quantum yields of **1a–d** are low or moderate in most solvents. In comparison, the fluorescence maxima of methoxybenzo[*b*]quinolizinium isomers **2a–d** do not shift as strongly as those of hydroxy-substituted derivatives **1a–d** in different solvents (Table 1). Although the emission bands of 8-methoxy-substituted derivative **2b** cover a somewhat larger range in different solvents, i.e. from 434 nm in 2-PrOH to 465 nm in DMSO, those of the other isomers **2a** and **2c** vary just slightly under the same conditions. The fluorescence quantum yields of the methoxy-substituted derivatives are about one order of magnitude larger than those of the hydroxy-substituted

Scheme 2. Synthesis of 7-Hydroxybenzo[*b*]quinolizinium (1a)

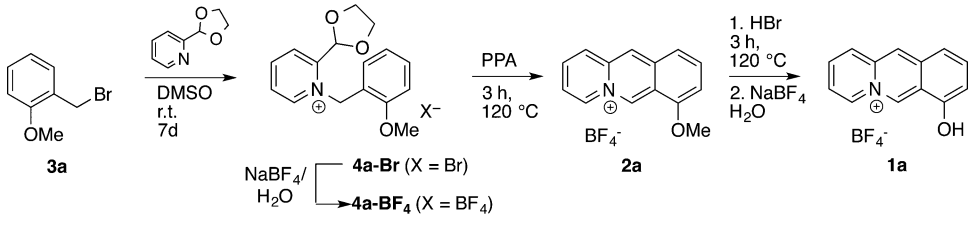

DOI: 10.1021/acs.joc.6b01991
J. Org. Chem. 2016, 81, 10942–10954

Table 1. Absorption and Emission Maxima and Fluorescence Quantum Yields, Φ_F, of 1b−d and 2b−d

solvent	λ_{abs}[a] (λ_{abs}[b])/nm	λ_{em}[c]/nm	λ_{em}[d]/nm	Φ_F[e]	$\lambda_{abs} - \lambda_{em}$/cm^{-1}[f]	λ_{abs}[a]/nm	λ_{em}[c] (Φ_F[e])/nm	$\lambda_{abs} - \lambda_{em}$/cm^{-1}[f]
	1a					**2a**		
H_2O	407, 492	501	-	<0.01	1241	371, 410	502 (031)	4470
MeOH	379, 423, (525)	504	-	<0.01	4844	373, 410	502 (0.28)	4470
EtOH	380, 428	504	-	<0.01	4461	374, 411	507 (0.29)	4607
1-PrOH	384, 430, (536)	504	-	<0.01	4703	374, 418	502 (0.29)	4003
2-PrOH	382, 442, (560)	503	-	<0.01	3792	374, 412	502 (0.18)	1230
CH_3CN	380, 426	504	-	<0.01	4571	373, 410	500 (0.29)	4390
DMSO	381, 424, (573)	515	-	<0.01	5370	376, 407	515 (0.26)	5153
DMF	442, 558	511	-	<0.01	3776	376, 408	511 (0.30)	4940
	1b					**2b**		
H_2O	357, (384)	597	-	0.02	11260	409	458 (0.22)	2616
MeOH	357, 390, (486)	630	484	0.01	12138	413	458 (0.15)	2379
EtOH	362, 398, (511)	634	485	0.02	11851	413	460 (0.19)	2474
1-PrOH	402, (498)	633	485	0.02	9077	415	434 (0.23)	1055
2-PrOH	409, (508)	635	484	0.02	8701	413	434 (0.18)	1172
CH_3CN	357, 419, (533)	-	468	0.08	6643	412	456 (0.14)	2342
DMSO	363, 428, (551)	654	504	0.01	12257	414	463 (0.12)	2557
DMF	362, 427, (549)	-	507	0.01	7900	n.d.	n.d.	n.d.
	1c					**2c**		
H_2O	385 (441)	527	-	0.29	6998	408	501 (0.49)	4550
MeOH	396 (453)	539	451	0.15	6768	409	505 (0.43)	4648
EtOH	402 (457)	544	-	0.05	6493	409	502 (0.47)	4530
1-PrOH	404 (460)	545	-	0.02	6365	408	501 (0.49)	4550
2-PrOH	383, 406 (462)	544	-	0.02	62481	409	505 (0.43)	4648
CH_3CN	378, 407 (469)	-	460	0.15	3428	409	502 (0.47)	4530
DMSO	378, 414 (478)	558	476	0.29	6234	408	501 (0.49)	4550
DMF	380, 416 (487)	556	475	0.15	6052	n.d.	n.d.	n.d.
	1d					**2d**		
H_2O	382, 405, 484	526	-	0.05	5680	373	495 (0.77)	6608
MeOH	383, 418	509	-	<0.01	6463	375	496 (0.83)	6505
EtOH	383	544	-	<0.01	7727	375	496 (0.83)	6505
1-PrOH	383, 428	475	541	<0.01	7625	377	493 (0.65)	6241
2-PrOH	385	478	-	<0.01	5054	n.d.	n.d.	n.d.
CH_3CN	377	507	-	0.03	6801	394, 412,	456 (0.14)	3451
DMSO	384, 469, 578	528	-	<0.01	2383	394, 414	463 (0.12)	3782

[a]Absorption maximum with lowest energy, $c = 10^{-4}$ M. [b]Absorption of broad red-shifted shoulder. [c]Dual emission: Red-shifted emission maximum, [d]Dual emission: Blue-shifted emission maximum, $c = 10^{-5}$ M, λ_{ex} = 404 nm (**1b**), 409 nm (**2b**), λ_{ex} = 378 nm (**1c**) and 410 nm (**2c**). [e]Relative fluorescence quantum yield relative to coumarin 1 (Φ_F = 0.73 in EtOH); estimated error: ±10% of the given values. [f]Difference between absorption maximum and emission maximum at lowest energy. [g]n.d. = not determined.

quinolizinium derivatives (Table 1), which indicates the radiationless deactivation of the excited states of **1a−d** due to specific interactions of the hydroxy group with the solvents.

Acid−Base Titrations. The absorption spectra of **1a−d** were determined at different pH values in a Britton−Robinson buffer.[18] As a general trend, the absorption and emission properties of hydroxybenzo[*b*]quinolizinium derivatives **1a−d** depend significantly on the pH of the solution (Figure 2A). For example, with increasing pH value of the solution from pH 2 to 10, the initial absorption bands at 374 nm (**1c**) and 377 nm (**1d**) decreased, whereas new red-shifted bands developed with maxima at 388 nm (**1c**) and 408 nm (**1d**), both of which are accompanied by a marked broad shoulder around 440 and 478 nm, respectively (positions of absorption maxima obtained by deconvolution of spectra). In most cases, isosbestic points were formed and maintained at lower pH values, whereas at alkaline conditions the isosbestic points vanished. The reversibilty of the prototropic reaction was demonstrated exemplarily for isomer **1b** by consecutive protonation and deprotonation (cf. Supporting Information, Figure S12).

In remarkable contrast to the absorption properties, the emission spectra of derivatives **1a−d** do not change much between pH 2 and pH 10. But notably, the fluorescence bands of these compounds diminish at very strong acidic conditions, e.g. on addition of aq $HClO_4$, with the formation of a blue-shifted emission band (Figure 2B). Thus, at higher concentration of $HClO_4$, the weak original emission band disappeared, whereas a new emission, in the case of **1b**[14] and **1c** with a strong blue shift, developed with an increase of the intensity by a factor of 72 for **1b**[14] and 11 for **1c**. It should be mentioned that in the case of **1a** and **1d** the shifts of the fluorescence maxima fluctuate with rising $HClO_4$ concentrations with no obvious trend.

The relationship of absorption and emission bands was further examined by fluorescence excitation spectra (Supporting Information, Figure S13). Thus, the shape and position of the absorption bands of derivatives **1a−d** essentially match the fluorescence excitation spectra of these compounds under acidic conditions as determined from monitoring the respective short-wavelength emission maximum (Supporting Information,

DOI: 10.1021/acs.joc.6b01991
J. Org. Chem. 2016, 81, 10942−10954

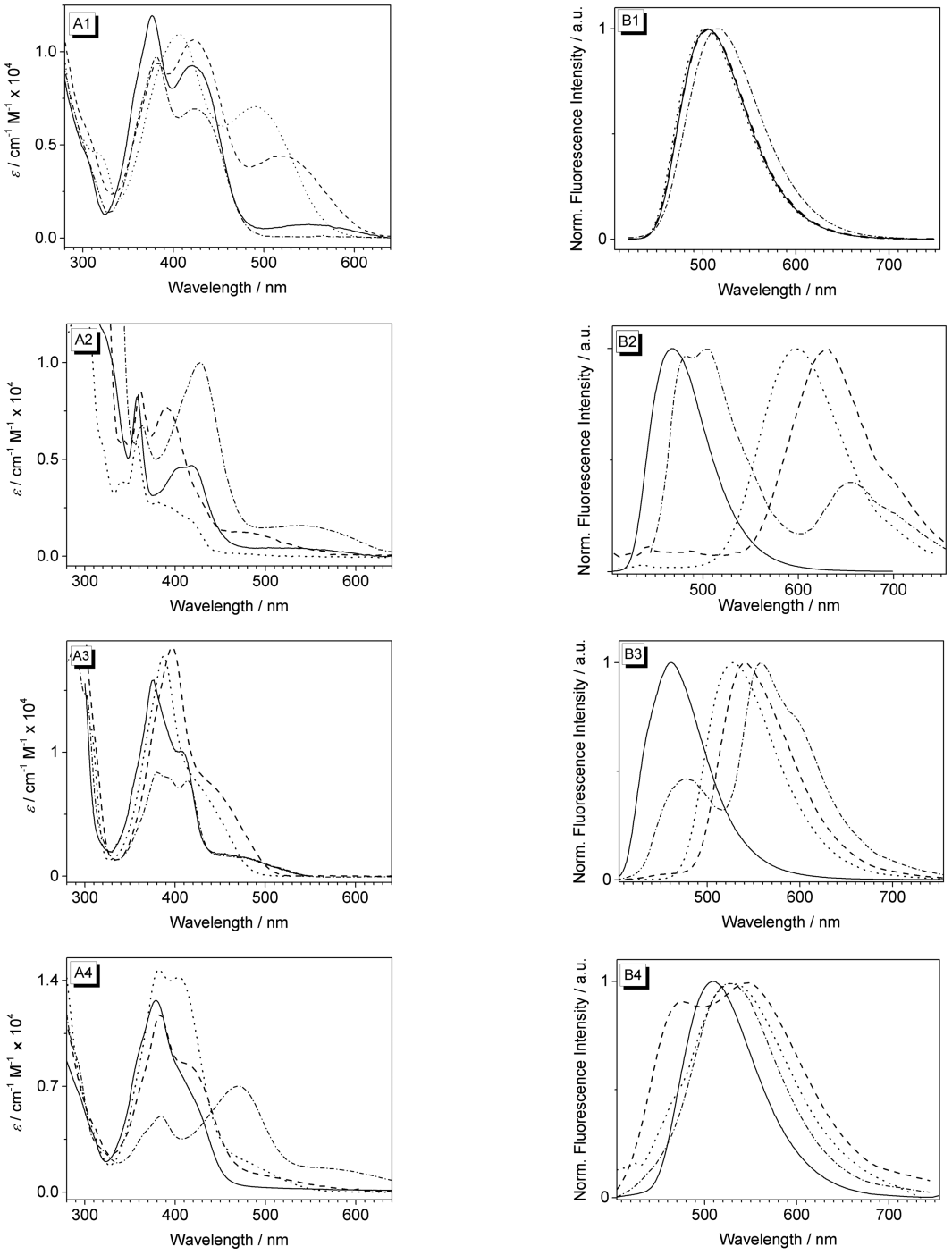

Figure 1. Absorption (A) and normalized fluorescence spectra (B) of **1a** (1), **1b** (2), **1c** (3) and **1d** (4) in different solvents (solid line: MeCN; dashed line: MeOH; dotted line: H_2O; dashed-dotted line: DMSO; c = 10 μM, respectively). Fluorescence spectra were recorded with excitation at the maximum of the long-wavelength absorption.

Figure S13). Accordingly, the excitation spectra of isomers **1b** and **1c** under alkaline conditions, monitored at the red-shifted emission maximum, resemble the absorption spectra under the same conditions. In the case of **1a** and **1d**, meaningful excitation spectra could not be observed from alkaline solutions, as the emission intensity is too low.

The acidity of the hydroxy-substituted benzo[*b*]quinolizinium derivatives in the ground and excited state was determined from the photometric and fluorimetric titrations in water. The pK_a values of compounds **1a**–**d** were determined by a numerical fit of the experimental data with the Henderson–Hasselbalch equation[19] (Figure 2). The pK_a* values were estimated according to the Förster-cycle considerations[20] (cf. Supporting Information). The pK_a and pK_a* values as well as the absorption and emission maxima at acidic and alkaline conditions are listed in Table 2. In the ground state, all four derivatives **1a**–**d** have moderate acidity with pK_a values in the range of 6.3–7.3. In the excited state, however, the 7-, 8-, and 9-hydroxybenzo[*b*]quinolizinium **1a**, **1b**, and **1c** are significantly more acidic as indicated by a low pK_a* of −1, 0, and −1. Unfortunately, the pK_a* of 10-hydroxy-substituted isomer **1d**

DOI: 10.1021/acs.joc.6b01991
J. Org. Chem. 2016, 81, 10942–10954

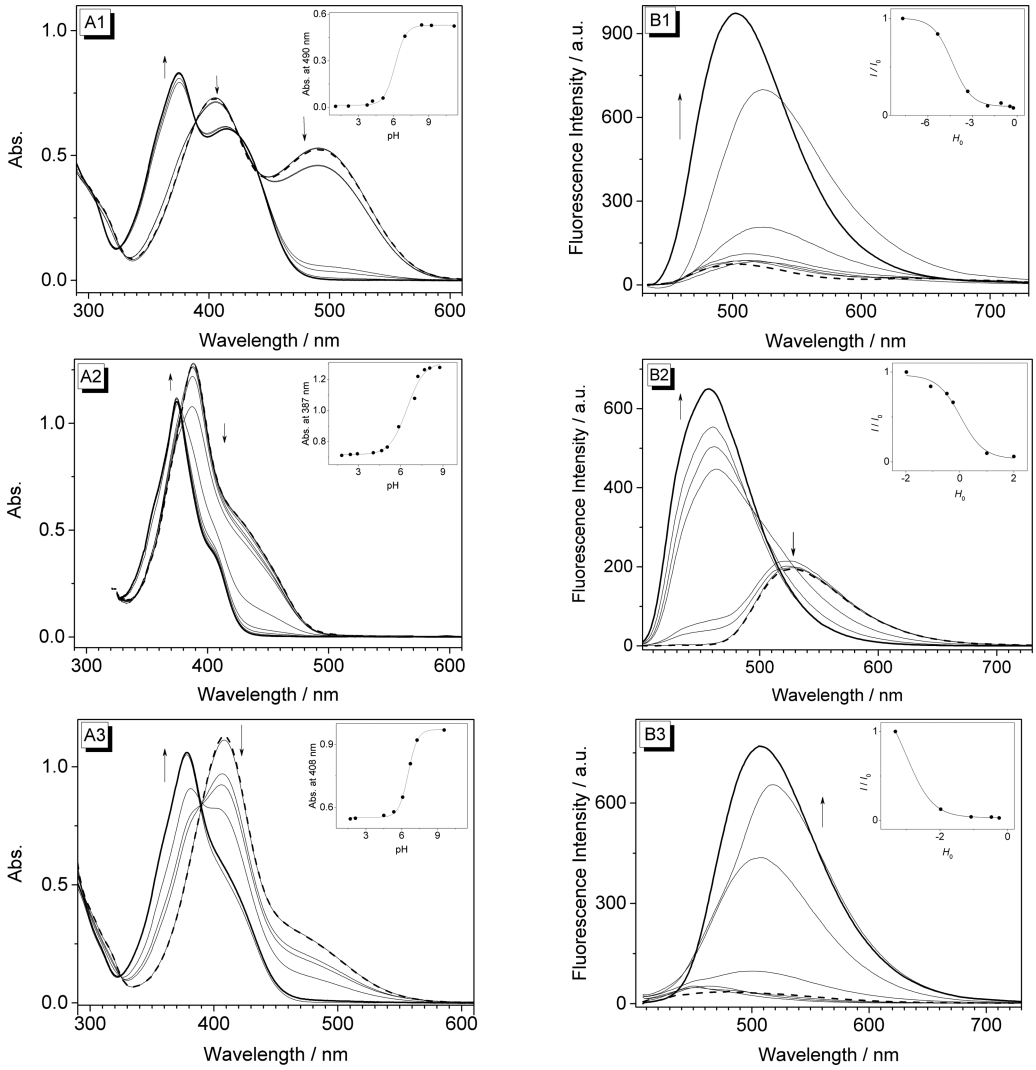

Figure 2. (A) Spectrophotometric titration of compounds **1a**, **1c**, and **1d** (1−3) with HCl (2 M) and NaOH (2 M) in Britton−Robinson buffer (c = 10^{-4} M). (B) Fluorescence spectra of **2a** (B1, λ_{ex} = 442 nm), **2c** (B2, λ_{ex} = 375 nm), and **2d** (B3, λ_{ex} = 389 nm) in $HClO_4$ of varied concentration (c = 10^{-5} M). Inset: Dependence of fluorescence intensity ratios from the concentration of the perchloric acid, characterized by Hammet acidity values H_0.[23] Arrows indicate changes in the spectra upon acidification. The dashed lines indicate spectra at the highest pH, and continuous bold lines indicate spectra at the lowest pH, respectively.

Table 2. pH-Dependance of Absorption and Fluorescence Maxima and pK_a and pK_a* values of 1a−d

	λ_{abs} (pH < 7)/nm	λ_{abs} (pH > 7)/nm[a]	λ_{em} (pH < 7)/nm	λ_{em} (pH > 7)/nm[c]	pK_a[d]	pK_a*[e]
1a	375, 416	401, 493	501	n.d.	7.3	−1
1b	338, 357, 398	371, 459	463	596	7.0	0
1c	374	386, 440	448	527	6.3	−1
1d	379	406, 478	476	n.d.	6.6	n.d.

[a]Absorption maximum in Britton−Robinson buffer determined by deconvolution analysis of the absorption bands, c = 10^{-4} M. [b]Fluorescence maximum in aq $HClO_4$ (11.8 M), c = 10^{-5} M, (**1a**: λ_{ex} = 442 nm; **1b**: λ_{ex} = 378 nm; **1c**: λ_{ex} = 375 nm, **1d**: λ_{ex} = 389 nm). [c]Fluorescence maximum in aq NaOH (0.1 M), c = 10^{-5} M. [d]pK_a value calculated according to the Henderson−Hasselbalch equation (ref 20), estimated errors: ±10% of the given values. [e]pK_a* value calculated according to Förster cycle (ref 21); estimated errors: ±10% of the given values.

could not be determined unambiguously because of the very weak and inconclusive emission of the deprotonated form.

For comparison, absorption and emission spectra of compounds **1b** and **1c** were also determined in methanol solution in the presence of acid or base (Figure 3). The absorption and fluorescence spectra of **1b** and **1c** did not change significantly in alkaline MeOH solution as compared to the neutral solution; namely the intensity of the bands just varies slightly in the different media. In contrast, acidification of the methanol solution led to a strong blue shift of the absorption bands of about $\Delta\lambda$ = 20−30 nm (Figure 3). Notably, a similar development of absorption bands was observed on dilution of methanol or acetonitrile solutions of the hydroxyhetarene **1c** *without* addition of acid or base (Supporting Information, Figure S10). Thus, upon incremental dilution of solutions of the derivative **1c**, the initial absorption band, that corresponds to the one in acidified medium, developed into a much broader unstructured band and

DOI: 10.1021/acs.joc.6b01991
J. Org. Chem. 2016, 81, 10942−10954

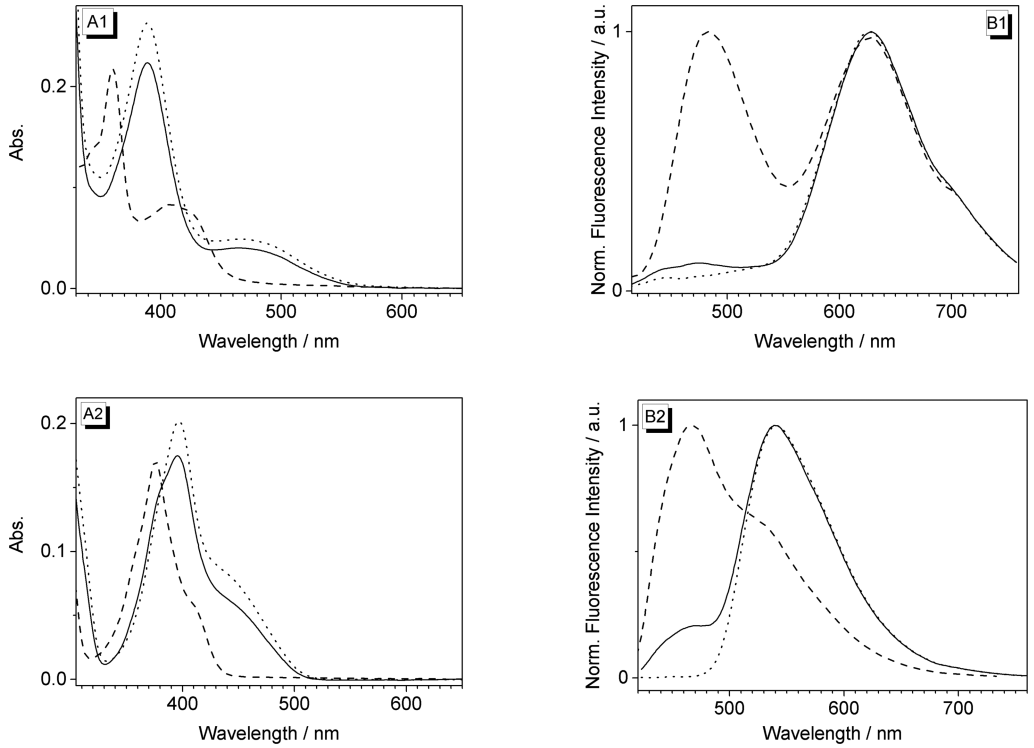

Figure 3. Absorption (A) and fluorescence spectra (B) of **1b** (1) and **1c** (2) in methanol (solid line), in acidified methanol solution (dashed line, addition of 20 μL of 2 M aq HCl), and in alkaline methanol solution (dotted line, addition of 20 μL of 1 M aq NaOH); c = 10 μM, λ_{ex} = 360 nm (**1b**)/390 nm (**1c**).

Table 3. Calculated Dipole Moments and Lowest-Energy Electronic Transitions of 1a–d and 1a^{cB}–d^{cB} from TD-DFT Calculations (CAM-B3LYP/D95 V) in Vacuo

	dipole moments μ (D)		electronic transitions					
	S_0	S_1	transition	λ_{max}/nm	oscillator strength f	q_{CT}	D_{CT}/Å	main contribution
1a	1.18	2.16	$S_0 \rightarrow S_1$	379	0.1204	0.54	1.24	HOMO → LUMO
			$S_0 \rightarrow S_2$	321	0.2099	n/a[a]	n/a	HOMO → LUMO+1
1a^{cB}	7.94	5.16	$S_0 \rightarrow S_1$	502	0.0803	0.61	1.45	HOMO → LUMO
			$S_0 \rightarrow S_2$	397	0.2605	n/a	n/a	HOMO → LUMO+1
1b	2.80	0.50	$S_0 \rightarrow S_1$	380	0.0588	0.51	1.13	HOMO → LUMO
			$S_0 \rightarrow S_2$	315	0.1135	n/a	n/a	HOMO → LUMO+1
1b^{cB}	11.55	8.65	$S_0 \rightarrow S_1$	559	0.0416	0.65	1.03	HOMO → LUMO
			$S_0 \rightarrow S_2$	405	0.2415	n/a	n/a	HOMO → LUMO+1
1c	3.70	1.73	$S_0 \rightarrow S_1$	361	0.1252	0.44	1.05	HOMO → LUMO
			$S_0 \rightarrow S_2$	319	0.1618	n/a	n/a	HOMO → LUMO+1
1c^{cB}	10.93	7.11	$S_0 \rightarrow S_1$	447	0.0676	0.63	1.29	HOMO → LUMO
			$S_0 \rightarrow S_2$	372	0.0000	n/a	n/a	HOMO−1 → LUMO
1d	1.97	2.25	$S_0 \rightarrow S_1$	383	0.0912	0.53	1.40	HOMO → LUMO
			$S_0 \rightarrow S_2$	323	0.2363	n/a	n/a	HOMO → LUMO+1
1d^{cB}	10.08	6.49	$S_0 \rightarrow S_1$	624	0.0310	0.68	1.43	HOMO → LUMO
			$S_0 \rightarrow S_2$	450	0.3076	n/a	n/a	HOMO → LUMO+1

[a]Not analyzed.

eventually converged to a red-shifted band that has essentially the same structure as the one obtained at higher pH values, i.e. after addition of base (Supporting Information, Figure S10). Upon addition of acid or base, the dual emission of **1b** and **1c** in methanol solution changes with respect to the contribution of the bands to the overall spectrum. Thus, in alkaline methanol solution the short-wavelength emission band completely (**1b**) or almost (**1c**) disappeared, whereas the fluorescence maximum at 630 nm (**1a**) and 540 nm (**1b**) was maintained. In acidified methanol solution, however, derivative **1b** exhibits dual emission with essentially equally intense bands with maxima at 483 and 630 nm. In the case of isomer **1c** the short-wavelength emission at 457 nm is much more intense than the one at 540 nm. Moreover, the latter band is significantly blue-shifted relative to the one observed in neutral methanol. To examine whether the same effect occurs in alcohols in general, similar experiments were undertaken in homologous alkanols (Supporting Information, Figure S9). Hence, upon addition of TFA to solutions of **1b** and **1c** in EtOH, 1-PrOH, 2-PrOH, 1-pentanol, and 1-hexanol, a blue-shifted emission band develops

DOI: 10.1021/acs.joc.6b01991
J. Org. Chem. 2016, 81, 10942–10954

at the expense of the initial long-wavelength emission. Notably, the decrease of the latter is more pronounced with increasing length of the alkyl fragment.

Time-Resolved Emission Spectroscopy. Time-resolved emission decays of derivatives **1b** and **1c** were recorded in water at the respective emission maxima. In water solution, the fluorescence decays of **1b** and **1c** were monoexponential with lifetimes of 3.4 ± 0.2 ns and 8.0 ± 0.2 ns, respectively. For comparison, an emission lifetime of 16.7 ± 0.2 ns was determined for methoxy-substituted derivative **2c** in methanol solution.

Quantum Chemical Calculations. To understand the electronic transitions underlying the photophysical properties of hydroxybenzo[*b*]quinolizinium ions, the ground and excited states were analyzed by quantum chemical calculations. First, for each of compounds **1a**−**d** and their corresponding conjugated bases (**1a**^{cB}−**d**^{cB}), the ground-state geometry was optimized using density functional theory (DFT) with a hybrid CAM-B3LYP potential and a D95 V basis set. Using the ground-state geometries, TD-DFT calculations on the same level of theory were subsequently used to calculate the excited-state dipole moments, the energies of vertical electronic transitions, and the involved molecular orbitals, as well as the changes of electronic density ($\Delta\rho$) upon excitation. The degree of charge transfer associated with the $S_0 \rightarrow S_1$ electronic transitions was also estimated through the analysis of q_{CT} and D_{CT} values.[21] Briefly, the changes of the electron density upon excitation are approximated as a transfer of a point charge of a magnitude of q_{CT} over a distance D_{CT} (the distance between the barycenters of density increase and decrease functions); the larger values of q_{CT} and D_{CT} correspond to a more pronounced charge-transfer character of electronic transitions.

The results of in vacuo DFT calculations (Table 3) demonstrate that, in all cases, the protonated forms (**1a**−**d**) are characterized by rather weak dipole moments (1.2−3.7 D) in the ground state, and electronic excitation has only a slight effect thereon (increase by <1 D in the case of **1a** and **1d**, decrease by ≈2 D in the case of **1b** and **1c**). In contrast, the zwitterionic forms are strongly polar in the ground state (7.9−11.5 D), and excitation leads to a decrease of the dipole moment: by 2.7 and 2.9 D for **1a**^{cB} and **1b**^{cB}, and by 3.8 and 3.6 D for **1c**^{cB} and **1d**^{cB}, respectively. Finally, TD-DFT calculations predict the red-shift of the long-wavelength absorption maximum of the zwitterionic form, compared to the protonated species whose $S_0 \rightarrow S_1$ transitions are centered about 360−380 nm. This red shift is particularly pronounced in the case of **1d**^{cB} (λ = 624 nm) and **1b**^{cB} (λ = 559 nm) and is much less important in the case of **1c**^{cB} (λ = 447 nm).

The TD-DFT analysis demonstrates that, in all cases, the lowest-energy transition is characterized by a major contribution of HOMO and LUMO. Notably, the position of the hydroxyl substituent in **1a**−**d** has essentially no effect on the spatial distribution of frontier molecular orbitals (Figure 4). Also, in all four cases, deprotonation of the hydroxyl group does not significantly change the spatial distribution of HOMO and LUMO but increases the electron density on the oxygen atom. Electronic excitation leads to a significant decrease of electron density at the oxygen atom, as characterized by lower LUMO coefficients compared to HOMO (Figure 4) and electron density difference plots (Supporting Information, Figure S15), demonstrating the tendency of all derivatives to lose a proton in the excited state. The concomitant increase of the electron density on the aromatic chromophore is

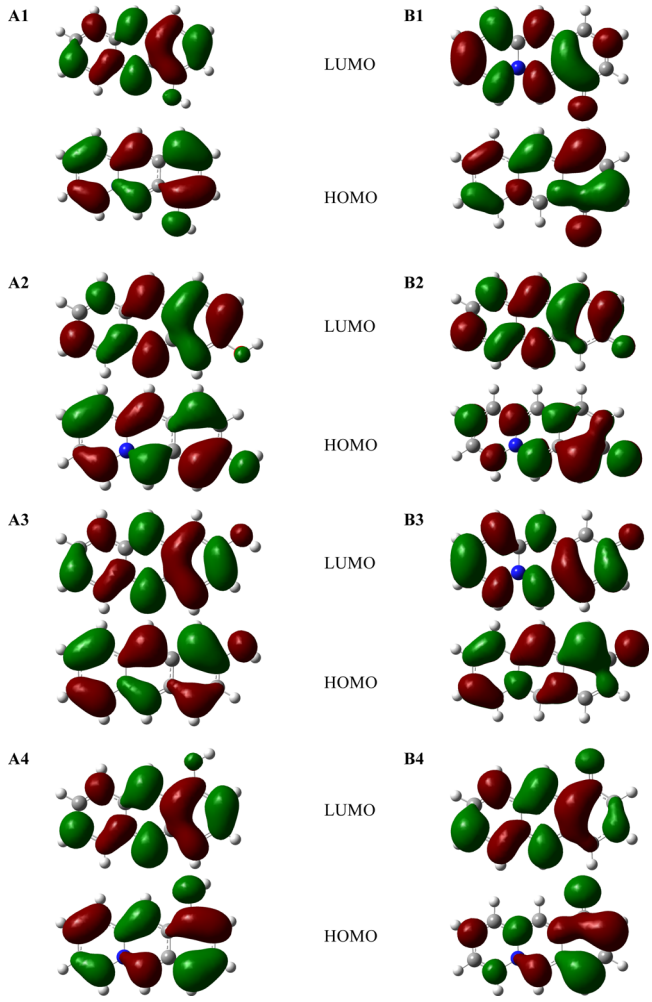

Figure 4. Plots of HOMO and LUMO (isovalue = 0.02) for **1a** (1), **1b** (2), **1c** (3), and **1d** (4, panel A) as well as the corresponding conjugated bases **1a**^{cB}−**d**^{cB} (panel B) from the gas-phase calculations. The wave function sign is arbitrary.

delocalized without significant preference for one or another atom (Supporting Information, Figure S15); that is, the electronic transitions do not show a particularly strong charge-transfer character. The latter point is also reflected in the q_{CT} and D_{CT} values (Table 3) that demonstrate that electronic transitions have a rather moderate charge-transfer character, which is slightly increased upon deprotonation of the hydroxyl group (q_{CT} = 0.6−0.7 for **1a**−**d**). Nonetheless, the charge-transfer distance does not exceed 1.5 Å, in accordance with rather small changes of dipole moments upon excitation. Quite remarkably, the results of quantum chemical calculations demonstrate that the photoacidity and the photophysical properties of hydroxybenzo[*b*]quinolizinium derivatives are essentially independent of the position of the hydroxyl substituent at the benzo[*b*]quinolizinium chromophore, i.e. no strong difference is observed between the conjugated (**1a**, **1c**) and cross-conjugated isomers (**1b**, **1d**).

To investigate the relative excited-state acidity of **1a**−**d** in aqueous solutions, more detailed calculations were performed. Following the methodology developed for similar systems,[22] the specific solvation effects were simulated by including a hydrogen-bonded cluster $(H_2O)_3$, and nonspecific solvent effects were included using the polarizable continuum model

DOI: 10.1021/acs.joc.6b01991
J. Org. Chem. 2016, 81, 10942−10954

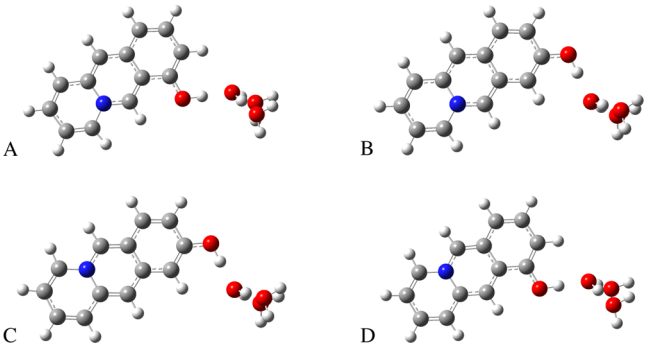

Figure 5. Clusters of **1a**$(H_2O)_3$ (A), **1b**$(H_2O)_3$ (B), **1c**$(H_2O)_3$ (C), and **1d**$(H_2O)_3$ (D) optimized in S_0 state in aqueous solution.

(CPCM). The geometries of clusters **1a**$(H_2O)_3$–**d**$(H_2O)_3$ were optimized in the ground state (Figure 5) and in the excited state (TD-DFT) using CAM-B3LYP/6-31+G(d,p) level of theory, and bond lengths and atomic charges were analyzed. The results (Table 4) demonstrate that, in all four cases, electronic excitation results in a decrease of the electron density at the oxygen atom, with a relative efficiency **1d** > **1a** > **1b** > **1c**. As a consequence, upon geometry relaxation, the O–O_w distance is decreased (following the same trend), demonstrating an increase of the hydrogen bond strength between the hydroxyl group and the acceptor water molecule. The C–O bond also significantly shortens following excitation, with most significant changes observed for **1d**$(H_2O)_3$ (0.088 Å) and least significant ones for **1c**$(H_2O)_3$ (0.045 Å). Again, no systematic influence of the substitution pattern (conjugated vs cross-conjugated) on the excitation-induced geometry changes was observed, consistent with the gas-phase calculations.

Notably, the vertical transition energies (absorption and emission) calculated for **1**$(H_2O)_3$ clusters are in excellent agreement with experimentally observed absorption spectra (in acidic conditions, cf. Table 2), demonstrating two maxima in the visible to near-UV spectral region which correspond to S_0–S_1 and S_0–S_2 transitions. Of particular note is a good agreement of emission wavelengths (corresponding to S_0–S_1 transitions) showing the reliability of the excited-state geometry calculations.

DISCUSSION

Acid–Base Equilbria. The photophysical studies of hydroxybenzo[*b*]quinolizinium derivatives **1a–d** clearly demonstrate that the absorption and emission properties of these compounds depend strongly on the solvent and the pH of the medium. In particular, all experimental data point to potential prototropic equilibria between the isomers **1a–d** and their conjugate bases **1a**^{cB}–**d**^{cB} in the ground and excited state, as clearly indicated by the pH-dependent absorption and emission properties in water and methanol (Figures 2 and 3). In general, the short-wavelength absorption and emission bands originate from the hydroxybenzo[*b*]quinolizinium, because these bands are predominant at acidic conditions. In addition, this assignment is supported in most cases by the fluorescence excitation spectra and by comparison with the resembling absorption and emission of methoxy-substituted derivatives **2a–d**, that cannot be deprotonated in the excited state (Supporting Information, Figure S11). As the only exception, the emission of **1c** at lower pH is significantly blue-shifted as compared with the one of **2c** in methanol. A comparison of the emission data of isomers **1a–d** and **2a–d** suggests that this discrepancy results from an "anomalous" emission energy of **1c** and may be the result of a pronounced, strong negative solvatochromic effect (see discussion below). At the same time, deprotonation of **1a–d** under alkaline conditions leads to the conjugate bases **2a**^{cB}–**d**^{cB} with significantly red-shifted absorption and fluorescence emission and excitation bands; however, the emission intensity is often very weak. This red-shift is most likely the result of the more pronounced donor–acceptor interplay between the substituent and the electron-accepting benzo[*b*]quinolizinium unit, because the oxyanion is a much better electron-donating substituent than the hydroxy functionality.[24] A similar red shift relative to the parent compound was observed for other donor-substituted quinolizinium derivatives, e.g. the analogous aminobenzo[*b*]-quinolizinium derivatives.[25] As the steady-state emission data clearly show that the hydroxybenzo[*b*]quinolizinium derivatives is almost completely deprotonated in the excited state and that the excited acid is only formed as emitting species under extreme acidic conditions, the detected emission lifetimes of **1b** and **1c** in the nanosecond range are assigned to the corresponding conjugate bases **1b**^{cB} and **1c**^{cB}.

Table 4. Main Structural Parameters, Atomic Charges, and Electronic Transitions for 1$(H_2O)_3$ Clusters in the S_0 State, Franck–Condon S_1 and S_2 States, and the Geometry-Optimized S_1 State from (TD-)CAM-B3LYP/6-31G+(d,p) Calculations

cluster	**1a**$(H_2O)_3$	**1b**$(H_2O)_3$	**1c**$(H_2O)_3$	**1d**$(H_2O)_3$
S_0 (Geometry-Optimized)				
d(O–O_w)/Å	2.575	2.598	2.584	2.590
d(C–O)/Å	1.335	1.338	1.332	1.339
δ(O)[a]	−0.756	−0.755	−0.745	−0.761
S_1 (Franck–Condon State)				
δ(O)[a]	−0.682	−0.693	−0.705	−0.684
λ_{max}[b]/nm (f[c])	409 (0.255)	390 (0.134)	369 (0.257)	407 (0.195)
S_2 (Franck–Condon State)				
λ_{max}[b]/nm (f[c])	342 (0.539)	326 (0.449)	331 (0.483)	346 (0.614)
S_1 (Geometry-Optimized)				
d(O–O_w)/Å	2.496	2.529	2.539	2.502
d(C–O)/Å	1.308	1.315	1.319	1.308
δ(O)[a]	−0.682	−0.695	−0.707	n.d.
λ_{max}[d]/nm	502	459	465	508

[a]Charge on the oxygen atom from Natural Population Analysis. [b]Absorption energy. [c]Oscillator strength. [d]Emission energy.

DOI: 10.1021/acs.joc.6b01991
J. Org. Chem. 2016, 81, 10942–10954

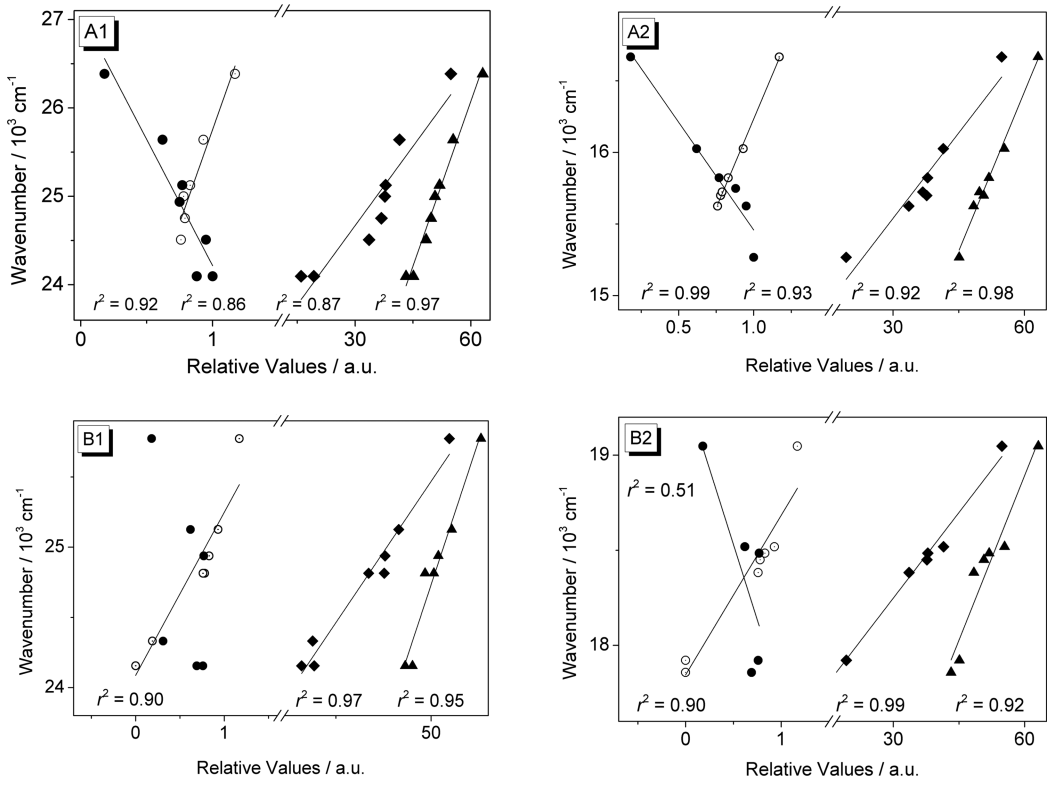

Figure 6. Plots of the absorption maxima (1) of **1b** (A) and **1c** (B) and emission maxima (2) of $\mathbf{1b}^{cB}$ (A) and $\mathbf{1c}^{cB}$ (B) versus solvent parameters β (●), $E_T(30)$ (▲), AN (◆), and α (○). The straight lines represent the linear fit of the experimental data.

It should be noted that the acid−base equilibrium depends also on the concentration of the hydroxyquinolizinium (cf. Supporting Information). This behavior is assumed to be caused by the interplay between the acid−base reaction and the different solubility of the components of this equilibrium, specifically as the deprotonation generates the charge neutral species $\mathbf{1c}^{cB}$ along with HBF_4 whose solubility in the applied solvents is supposed to be different from the one of the acid **1c** and its counterion. Thus, with increasing dilution, the fine balance between prototropic equilibrium and solubility of substrates and products is shifted toward deprotonation.

Hydroxybenzo[*b*]quinolizinium derivatives **1a**, **1b**, and **1c** exhibit a pronounced excited-state acidity, similar to compounds such as cyanonaphthol,[26] 8-hydroxypyrene-1,3,6-trisulfonate,[27] or hydroxyquinolinium[12b,13] derivatives whose pK_a values decrease by several orders of magnitude in the excited state. In fact, with low pK_a^* values around 0 these compounds fall into the type II category of photoacids,[10a] i.e. their excited-state acidity is sufficiently strong to protonate water and protic organic solvents such as alcohols. Although the pK_a^* value of derivative **1d** could not be determined, it is obvious from the formation of its emission bands only in the presence of strong acid (Figure 2) that this isomer has a photoacidity resembling that of derivatives **1a−c.** The photoacidity of hydroxyarene derivatives is well established[10] and mainly explained by a favorable photoinduced intramolecular charge transfer (ICT) from the hydroxy donor substituent to the arene unit. As a result, the excited molecule has an increased acidity because after deprotonation the negative charge of the oxyanion donor is well delocalized within the excited aromatic system. This mechanism, though highly simplified, was confirmed by the observation that several naphthol or phenol derivatives exhibit increasing acidity upon substitution of acceptor substituents that further increase the electron-accepting properties of the aromatic unit.[10,11] In analogy to these principles we propose that 8- and 9-hydroxybenzo[*b*]quinolizinium ions **1b** and **1c** also act as photoacids because the benzo[*b*]quinolizinium unit serves as a strong acceptor that supports the formation of the deprotonation to give $\mathbf{1b}^{cB}$ and $\mathbf{1c}^{cB}$ in the excited state, either by linear conjugation or cross-conjugation. This assumption is supported by the observation of a similar effect in cationic hydroxyhetarenes, e.g. in cationic pyridinium-based biaryl-type photoacids[28] or the highly photoacidic quinone-cyanine-9 dye.[29]

The quantum chemical calculations also support the photoacid behavior of hydroxybenzo[*b*]quinolizinium derivatives, as demonstrated by the decrease of the partial charge on the oxygen atom upon excitation (in vacuum or in water-bound clusters) which facilitates proton transfer, compared to the ground state. Notably, the geometry changes in the excited state predicted in water-bound clusters, namely the approach of the water molecule (hydrogen-bond acceptor) and shortening of the C−O bond, are qualitatively and quantitatively comparable to those computationally observed in the case of *N*-methyl-6-hydroxyquinolinium cation, a class III strong photoacid ($pK_a^* = -4$ to -6).[22] Thus, among the hydroxybenzo[*b*]quinolizinium derivatives, the isomer **1d** demonstrates the strongest charge-transfer and geometry changes upon photoexcitation, similar to those of *N*-methyl-6-hydroxyquinolinium, and the computed photoacidity strength decreases in the series **1d** > **1a** > **1b** > **1c**. Unfortunately, the relative photoacidity strength could not be confirmed experimentally due to significant approximations necessary for the determination of the experimental pK_a^* values.

Solvatochromism. To identify relationships between the absorption and emission properties of compounds **1b** and **1c**

DOI: 10.1021/acs.joc.6b01991
J. Org. Chem. 2016, 81, 10942−10954

and the solvent properties, the absorption and emission energies were plotted versus representative solvent parameters, namely the polarity [$E_T(30)$], the hydrogen-bond donor (HBD) or hydrogen-bond acceptor (HBA) properties (α, β), and the ability to stabilize negative charges (AN) (Figure 6).[30] In the case of derivative **1b**, a transition at higher energy, i.e. around 360 nm, was used for the analysis of the solvatochromism instead of the long-wavelength absorption band, because in most solvents the latter is too broad and a maximum cannot be determined unambiguously. With few exceptions, the absorption energies (in wavenumbers) of **1b** and **1c** correlate well with these solvent properties, especially with the solvent polarity (r^2 = 0.97 and 0.95, respectively). Namely, the absorption energy increases in solvents with higher polarity. This negative solvatochromism usually indicates a more pronounced stabilization of the ground state by dipole−dipole interactions between the solvent and the solute than in the excited state.[27,30] At the same time, the absorption energies of compounds **1b** and **1c** increase almost linearly (r^2 = 0.92 and 0.90, respectively) with the HBD properties, as characterized by the Kamlet−Taft parameter α of the protic solvents. This relationship denotes the significant stabilization of hydrogen bonds between the solvent and the oxygen atom of the hydroxy functionality that is more pronounced in the excited state than in the ground state. It should be emphasized, however, that absolute differences of absorption shifts are relatively small ($\Delta\lambda \leq 20$ nm), indicating that the differences in the stabilization of the ground and excited state by the solvent are not very large. This is in agreement with the relatively small changes of dipole moments of **1a**−**d** upon excitation (Table 4).

Hydroxybenzo[*b*]quinolizinium derivatives **1b** and **1c** display a pronounced fluorosolvatochromism that is caused by a combination of solvent−solute interactions and a prototropic equilibrium. The latter is an important factor, as hydroxyarenes **1b** and **1c** have an emission different from that of their conjugate bases $\mathbf{1b}^{cB}$ and $\mathbf{1c}^{cB}$, and the acid−base equilibrium is not the same in the different employed solvents. As a result, dual emission is observed that originates from emission of hydroxyarene derivatives **1b** and **1c**, along with one of their deprotonated forms $\mathbf{1b}^{cB}$ and $\mathbf{1c}^{cB}$ (see discussion above). Therefore, the assessment of the fluorosolvatochromic properties of the hydroxybenzo[*b*]quinolizinium isomers needs to consider both emitting forms **1b**,**c** and $\mathbf{1b}^{cB}$,$\mathbf{c}^{cB}$ and differentiate between them. In general, the emission energies of hydroxyquinolizinium derivatives **1b** and **1c** do not correlate well with solvent parameters such as $E_T(30)$, α, β, AN, or DN. Apparently, the emission properties of these compounds are significantly influenced by several of these parameters with different trends and to different extents. Unfortunately, a multiparameter approach to dissect the different solvent effects was hampered by the limited solubility of derivatives **1b** and **1c**, that did not allow us to employ a larger series of different solvents. In contrast, the emission energies of the conjugate bases $\mathbf{1b}^{cB}$ and $\mathbf{1c}^{cB}$ correlate well (r^2 = 0.90−0.99) with most of the tested solvent parameters. Specifically, the emission energies, as quantified by the wavenumber, increase with decreasing solvent polarity [$E_T(30)$] and polarizability (π) or with H-bond donating or anion-stabilizing properties of the solvent (α, AN). Especially the negative solvatochromism of **1b**, that corresponds to a hypsochromic shift of the emission maximum with increasing solvent polarity, may be explained by a charge transfer in the excited state that is also responsible for the negative fluorosolvatochromism of several structurally resembling merocyanines,[31] such as oxidostilbazonium derivatives,[32] as well as *N*-methyl-6-hydroxyquinolinium.[13] The negative solvatofluorochromism observed with **1b** and **1c** is in line with the lower excited-state dipole moments of **1b** and **1c**, and particularly their conjugated bases, compared to the ground state, as shown by the DFT calculations (Table 4). Hence, the excited state has a significantly smaller dipole and experiences a less pronounced stabilization by polar solvents than the ground state. Thus, with increasing polarity of the solvent, the ground state is increasingly stabilized, leading to a larger HOMO−LUMO gap and in turn a bathochromic shift of the absorption and emission maximum. It should be noted that this effect occurs when the oxyanion and the pyridinium unit are both in a conjugated ($\mathbf{1c}^{cB}$) and in a cross-conjugated arrangement ($\mathbf{1b}^{cB}$); therefore, the VB-description of the ground and excited states in terms of a "quinoid" structure is not appropriate for explanation of electronic transitions in this series. Contrary to **1b** and **1d**, the emission of the isomer **1a** originates exclusively from the protonated form and shows little solvatofluorochromism (Figure 1, B1), which is likely due to a small difference of the dipole moment between the S_0 and S_1 states in this case (<1 D, Table 4). A similarly small change of dipole moment is observed for **1d**; however, in the latter case, the observed moderate fluorosolvatochromism is likely due to the contribution from the deprotonated species ($\mathbf{1d}^{cB}$).

Although the fluorosolvatochromism of $\mathbf{1b}^{cB}$ and $\mathbf{1c}^{cB}$ may be explained by the effect of solvent polarity on the emission properties, the influence of the H-bond-donating or anion-stabilizing properties of the solvent appears to be significant as well, because both corresponding solvent parameters, α and AN, correlate well with the emission energies of $\mathbf{1b}^{cB}$ and $\mathbf{1c}^{cB}$ ($r^2 \geq 0.96$). This observation is in agreement with the postulated electron distributions in the ground and excited states (Figure 4). In this instance, solvents that stabilize the oxyanion functionality in $\mathbf{1c}^{cB}$ lower, in analogy to the stabilization by polar solvents, the energy of the ground state, whereas this effect does not operate in the excited state, thus leading to the blue shift of the emission maximum with increasing α and AN values.

To conclude, the combination of acidochromic and solvatochromic properties provides a broad range of medium-dependent emission colors of hydroxybenzo[*b*]quinolizinium derivatives **1b**−**d** (Figure 7). To be noted is the fact that this type of solvatochromism may be effectively used in fluorimetric chemosensors,[33] specifically as the benzo[*b*]quinolizinium ion is a useful fluorescent platform for such functional dyes.[15] Hence, in a typical experiment the benzo[*b*]quinolizinium is

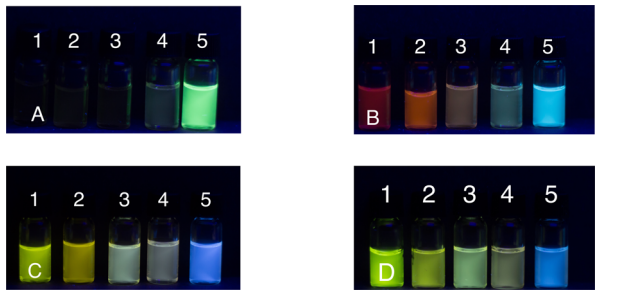

Figure 7. Pictures of the emission colors of hydroxybenzo[*b*]-quinolizinium derivatives **1a** (A), **1b** (B), **1c** (C), and **1d** (D), in H_2O (1), MeOH (2), 2-PrOH (3), DMSO (4), and MeCN (5) with UV light excitation ($c = 10^{-4}$ M; λ_{ex} = 366 nm).

DOI: 10.1021/acs.joc.6b01991
J. Org. Chem. 2016, 81, 10942−10954

Scheme 3. Design of Fluorescent Chemosensors Based on 9-Hydroxybenzo[*b*]quinolizinium (1c)

functionalized with a substituent X that is selectively transformed into a hydroxy group in the presence of the analyte (Scheme 3). If the substituent X has no strong electron-donating or -accepting properties, the emission of the substrate should fall into the typical range of benzo[*b*]quinolizinium derivatives, i.e. around 420 nm.[15] Upon treatment with the analyte, the hydroxy-substituted derivative is formed, leading to a red-shifted emission at 527 nm (in water). Thus, the change of the emission maximum may be used to detect the analyte qualitatively or even quantitatively. The substituent X may be an ether or ester functionality that produces the hydroxy group upon metal- or enzyme-catalyzed cleavage, so that the catalyst or enzyme is the analyte. In another approach, X could be a boronic acid (ester) or sulfonate that is oxidized to the hydroxy group. Indeed, we have already demonstrated, based on this concept, that boronobenzo[*b*]quinolizinium can be used for the ratiometric fluorimetric detection of hydrogen peroxide, even in living cells.[34]

CONCLUSIONS

In summary, we have demonstrated that hydroxy-substituted benzo[*b*]quinolizinium derivatives represent a novel class of water-soluble solvatochromic photoacids. All experimental and theoretical studies point to strong acidity of these compounds in the excited state. On the basis of the low pK_a* values <0, these compounds are categorized as type II photoacids, that are strong enough to protonate water as well as alcohols. Most notably, the combination of the prototropic properties of hydroxybenzo[*b*]quinolizinium with the particular solvent–solute interactions of the acid and its conjugate base in the excited state leads to a pronounced fluorosolvatochromism that covers a broad range of emission colors. From these observations we conclude that hydroxy-substituted benzo[*b*]-quinolizinium derivatives represent a promising class of organic photoacids that may be used either as water-soluble fluorescent probes, based on their pronounced solvatochromism, or as water-soluble sources for photoinduced generation of acids, e.g. to catalyze organic reactions. For example, the acid-catalyzed deprotection of alcohols or the acid–based initiation of polymerization reactions shall be investigated in future studies.

EXPERIMENTAL SECTION

General Instrumentation and Materials. All commercially available chemicals were reagent grade and used without further purification. 8-Methoxybenzo[*b*]quinolizinium tetrafluoroborate (**2b**),[17d] 8-hydroxybenzo[*b*]quinolizinium bromide (**1b**),[17d] 9-methoxybenzo[*b*]quinolizinium tetrafluoroborate (**2c**),[17b] and 9-hydroxybenzo[*b*]quinolizinium tetrafluoroborate (**1c**)[17a] were prepared according to literature procedures. The melting points are not corrected. ESI mass spectra were recorded in the positive-ion mode, source voltage 6 kV; only *m*/*z* values in the range of 100–2000 units were analyzed. NMR spectra were measured at 400 MHz (^{1}H) and 100 MHz (^{13}C) at 20 °C; chemical shifts are given in ppm (δ) relative to TMS (δ = 0.00 ppm). Unambiguous proton NMR assignments were established by {1H, 1H}-COSY, HSQC, and HMBC experiments.

Synthesis. *2-(1,3-Dioxolan-2-yl)-1-[2-methoxybenzyl]pyridinium Tetrafluoroborate (**4a-BF$_4$**).* A solution of 2-(bromomethyl)anisole[35] (36.5 mmol) and 2-(1,3-dioxolan-2-yl)pyridine[36] (7.31 g, 48.4 mmol) in DMSO was stirred for 7 days at room temperature. The reaction mixture was poured into EtOAc. The white precipitate was collected, washed with EtOAc and diethyl ether, and dried in vacuo to give the product **4a-Br** as a white solid. The solid was dissolved in a minimal amount of water, and a saturated aqueous solution of $NaBF_4$ was added. The precipitate was recrystallized from MeCN/EtOAc to give **4a-BF$_4$** (7.70 g, 61%) as a yellow crystalline solid; mp 89–91 °C. ^{1}H NMR (400 MHz, DMSO-d_6): δ = 3.76 (s, 3 H, OCH_3), 4.12 (s, 4 H, $CH(OCH_2)_2$), 5.93 (s, 2 H, CH_2), 6.55 (s, 1H, $CH(OCH_2)_2$), 7.02 (t, ^3J = 7 Hz, 1H, Ar–H), 7.13 (d, ^3J = 7 Hz, 1 H, Ar-H), 7.22 (dd, ^3J = 8 Hz, ^4J = 2 Hz, 1 H, Ar-H), 7.46 (t, ^3J = 8 Hz, 1H, Ar-H), 8.18 (t, ^3J = 8 Hz, 1 H, Ar-H$_{py}$), 8.31 (d, ^3J = 8 Hz, 1 H, Ar-H$_{py}$), 8.71 (t, ^3J = 8 Hz, 1 H, Ar-H$_{py}$), 8.90 (dd, ^3J = 6 Hz, ^3J = 1 Hz, 1 H, Ar-H$_{py}$). ^{13}C NMR (100 MHz, DMSO-d_6): δ = 55.7 (OCH_3), 56.4 (CH_2), 65.7 ($CH(OCH_2)_2$), 97.0 ($CH(OCH_2)_2$), 111.6 (CH), 120.9 (CH), 121.1 (C_q), 125.6 (CH), 128.4 (CH), 130.2 (CH), 131.2 (CH), 146.7 (CH), 147.1 (CH), 152.0 (C_q), 157.1 (C_q). $C_{16}H_{18}BF_4NO_3$ (359.1 g/mol); calcd: C 53.51, H 5.05, N 3.90; found: C 53.62, H 5.04, N 4.40. MS (ESI): *m*/*z* (rel inten) = 272 [M^+] (100).

*7-Methoxybenzo[b]quinolizinium Tetrafluoroborate (**2a**).* A solution of benzylpyridinium **4a-BF$_4$** (0.77 g, 2.14 mmol) in PPA (8 g) was slowly heated under argon atmosphere to 150 °C, and the reaction mixture was stirred at this temperature for 3 h. After cooling to 100 °C, water was added and the mixture was stirred at 150 °C for 30 min. CAUTION: Hydrolysis may be highly exothermic! The mixture was cooled to room temperature and treated with excess of $NaBF_4$ (saturated aqueous solution). The solution was extracted with nitromethane (3 × 20 mL). The organic layers were combined, washed with water, dried with Na_2SO_4, and evaporated in vacuo. The remaining residue was crystallized from MeOH/EtOAc to give the product as a yellow solid (0.12 g, 19%); mp >300 °C. ^{1}H NMR (400 MHz, DMSO-d_6): δ = 4.17 (s, 3 H, OCH_3), 7.36 (d, ^3J = 8 Hz, 2 H, 8-H), 7.87 (d, ^3J = 9 Hz, 1 H, 10-H), 7.91 (t, ^3J = 7 Hz, 1 H, 3-H), 8.04 (t, ^3J = 8 Hz, 2 H, 2-H, 9-H), 8.49 (d, ^3J = 9 Hz, 1 H, 1-H), 9.11 (s, 1 H, 11-H), 9.44 (d, ^3J = 7 Hz, 1 H, 4-H), 10.43 (s, 1 H, 6-H). ^{13}C NMR (100 MHz, DMSO-d_6): δ = 57.0 (OCH_3), 107.9 (C8), 118.9 (C10), 119.8 (C_q), 122.2 (C3), 124.2 (C11), 126.8 (C1), 131.7 (C9), 135.1 (C_q), 136.3 (C4), 136.5 (C6), 136.6 (C2), 138.0 (C_q), 155.1 (C_q). $C_{14}H_{12}BF_4NO$ (297.1 g/mol); calcd: C 56.61, H 4.07, N 4.72; found: C 56.63, H 4.35, N 4.28. MS (ESI): *m*/*z* (rel inten) = 210 [M^+] (100).

*7-Hydroxybenzo[b]quinolizinium Tetrafluoroborate (**1a**).* A solution of **2a** (300 mg, 1.00 mmol) in aq HBr (48%) (5 mL) was stirred at 90 °C for 4.5 h. The reaction mixture was cooled to room temperature, and the solvent was removed in vacuo. The residue was dissolved in water and treated with excess of $NaBF_4$ (saturated aqueous solution). The precipitated yellow solid was isolated and recrystallized from methanol to give the product (100 mg, 41%) as a yellow solid; mp 210–216 °C. ^{1}H NMR (400 MHz, DMSO-d_6): δ = 7.21 (d, ^3J = 4 Hz, 1 H, 8-H), 7.78 (d, ^3J = 4 Hz, 1 H, 10-H), 7.85 (t, ^3J = 7 Hz, 1 H, 3-H), 7.97 (t, ^3J = 7 Hz, 2 H, 2-H, 9-H), 8.45 (d, ^3J = 9 Hz, 1 H, 1-H), 9.05 (s, 1 H, 11-H), 9.39 (d, ^3J = 7 Hz, 1 H, 4-H), 10.44 (s, 1 H, 6-H). ^{13}C NMR (100 MHz, DMSO-d_6): δ = 110.4 (C10), 116.7 (C7), 119.4 (Cq), 121.3 (C4), 123.5 (C6), 126.4 (C5), 130.5 (C9), 134.4 (C3), 136.1 (Cq), 136.7 (C8), 136.9 (C1), 136.9 (Cq), 156.1 (Cq). $C_{13}H_{10}BF_4NO\cdot{}^1/_4Et_2O$ (301.55 g/mol); calcd: C 55.76,H 4.18, N 4.64; found: C 55.90, H 3.97, N 4.61 $C_{13}H_{10}BF_4NO$ (283.1 g/mol); calcd: C 55.17, H 3.56, N 4.95; found: C 55.01, H 3.19, N 5.14. MS (ESI): *m*/*z* (rel inten) = 196 [M^+] (100).

*10-Hydroxybenzo[b]quinolizinium Tetrafluoroborate (**1d**).* A solution of **2d**[17b] (645 mg, 2.17 mmol) in aqueous HBr (48%) (15 mL) was stirred at 100 °C for 24 h. The reaction mixture was cooled to room temperature, and the solvent was removed in vacuo. The residue was dissolved in water and extracted with $MeNO_2$ (3 × 20 mL). The solvent was evaporated, the residue was dissolved in a small

DOI: 10.1021/acs.joc.6b01991
J. Org. Chem. 2016, 81, 10942–10954

amount of water and treated with an excess of $NaBF_4$ (saturated aqueous solution). The precipitated yellow solid was isolated and recrystallized from 2-PrOH to give the product (188 mg, 31%) as a yellow solid; mp 172−176 °C. ^{1}H NMR (400 MHz, DMSO-d_6): δ = 7.32 (dd, ^3J = 7 Hz, 1 H, 4-H), 7.85 (m, 2 H, 1-H, 3-H), 7.92 (ddd, ^3J = 7 Hz, 1 H, 8-H), 8.02 (t, ^3J = 8 Hz, 1 H, 2-H), 8.65 (d, ^3J = 9 Hz, 1 H, 9-H), 9.21 (d, ^3J = 7 Hz, 1 H, 7-H), 9.28 (s, 1 H, 11-H), 10.31 (s, 1 H, 6-H), 11.61 (s, 1H, OH). ^{13}C NMR (100 MHz, DMSO- d_6): δ = 113.6 (C4), 117.9 (C3), 120.3 (C11), 122.5 (C8), 126.9 (Cq), 127.3 (C9), 128.4 (Cq), 130.3 (C2), 132.3 (C7), 136.8 (Cq), 139.3 (C6), 139.3 (C6), 152.6 (C10). C $_{13}H_{10}BF_4NO$ (283.1 g/mol); calcd: C 55.17, H 3.56, N 4.95; found: C 54.82, H 3.42, N 4.74. MS (ESI): m/z (rel inten) = 196 [M^+] (100).

Absorption and Emission Spectroscopy. Absorption spectra were recorded on a double beam spectrometer in quartz cells (10 mm × 10 mm) with baseline correction. Absorption spectra were collected with a detection speed of 120 nm/min in a range from 300 to 750 nm. The absorption maxima of the hydroxyquinolizinium ions and their deprotonated forms were determined by deconvolution analysis of the absorption bands. Fluorescence emission spectra were collected in quartz cells (10 mm × 10 mm) with baseline correction. The excitation and emission slits were adjusted to 5 nm bandwidths. The voltage was adjusted according to the emission intensity of the sample between 400 and 800 V.

Solutions were freshly prepared for each measurement from stock solutions in a suitable solvent (c = 1.0 × 10^{-3} M). For experiments in different solvents, aliquots of the stock solution were evaporated and redissolved in the respective solvent. Unless mentioned otherwise, measurements were performed at 20 °C in deionized water (resistivity ≤18 MΩ cm), methanol (HPLC grade, water content: 0.002%), acetonitrile (HPLC grade, water content: 0.03%), or anhydrous solvents. The formation of aggregates was excluded by checking consistent absorption, excitation, and fluorescence spectra of the samples in different solvents (CH_3CN, MeOH, H_2O) at varying concentrations (2 μM to 80 μM).

The relative fluorescence quantum yields were determined under identical conditions with the same settings on the spectrometer (detection wavelength, excitation wavelength, slit bandwidths, collection rate). Fluorescence quantum yields were determined with Coumarin 1 (Φ_{FL} = 0.73 (EtOH))[37] as the standard. The emission spectra were collected from solutions whose concentration was adjusted such that A = 0.1. After integration of the fluorescence band (I), the relative fluorescence quantum yields were calculated according to eq 1.

$$\Phi_{FL} = \frac{I_{FL}}{I^S_{FL}} \frac{n^2}{n^2_S} \Phi^S_{FL} \quad (1)$$

where I_{Fl} and I^S_{FL} are the emission intentsities of the sample and the standard, and n^2 and n^2_S are the refractive indices of the sample solution and the standard solution.

For the determination of the pK_a value, the Britton−Robinson buffer solution was prepared according to a known procedure from phosphoric acid, boric acid, and sodium acetate (0.04 M each) in water and adjusted to pH = 7.0 by the addition of an aqueous solution of NaOH (2 M).[18] The sample was dissolved in the buffer solution (c = 1.0 × 10^{-4} M), and subsequently aliquots of aq HCl (2 M) or NaOH (2 M) were added. After each addition step, the pH and the absorption spectra were determined. The titrations were performed in a pH range between 9 and 1. For further analysis, the absorption maxima were plotted versus the pH of the solution, and the acidity constant pK_a was obtained by numerical fitting of the experimental data to the Henderson−Hasselbalch equation.[20]

For the determination of the pK_a* values, the emission spectra were determined from samples (c = 1.0 × 10^{-5} M) that were dissolved in solutions with different $HClO_4$ concentrations (0.01−11.8 M). The emission intensity was plotted versus the Hammet acidity values H_0[19] of the solution. The pK_a* values were calculated from the absorption and fluorescence data according to the Förster-cycle.[21]

Fluorescence decays were recorded with an Edinburgh Instruments OB920 single photon counter (SPC). As a source of light, a laser diode with λ_{ex} = 378 nm (**1b**, **1c**, **2c**) was used. The instrument response function (IRF) was collected using a Ludox solution at the excitation wavelengths. Data analysis was performed with either deconvolution or tail fitting with F900 and Fast software. The fits were considered adequate when the residuals between the experimental and calculated values were random and the χ^2values were between 0.9 and 1.2.

■ ASSOCIATED CONTENT

Supporting Information

The Supporting Information is available free of charge on the ACS Publications website at DOI: 10.1021/acs.joc.6b01991.

NMR spectra of compounds **4a-BF$_4$**, **2a**, **1a**, and **1b**; absorption and emission spectra in different media; determination of pK_a* values; computational studies (PDF)

■ AUTHOR INFORMATION

Corresponding Author

*Tel: 49 (0) 271 740 3440. E-mail: ihmels@chemie.uni-siegen.de.

Notes

The authors declare no competing financial interest.

■ ACKNOWLEDGMENTS

This paper is dedicated to Prof. Dr. Gerhard Bringmann on the occasion of his 65th birthday. This work was generously financed by the Deutsche Forschungsgemeinschaft (IH24/10-1). The authors at the University of Victoria thank the Natural Science and Engineering Research Council Canada for financial support (RGPIN-121389-2012). We thank Mr. H. Bodenstedt (Organische Chemie I, Universität Siegen) for performing elemental microanalysis. A.G. acknowledges the access to the Cloud@VD platform provided by the Université Paris Sud.

■ REFERENCES

(1) *Acid Catalysis in Modern Organic Chemistry*; Yamamoto, H., Ishihara, K., Eds.; Wiley-VCH: Weinheim, 2008.

(2) Manallack, D. T.; Prankerd, R. J.; Yuriev, E.; Oprea, T. I.; Chalmers, D. K. *Chem. Soc. Rev.* **2013**, *42*, 485.

(3) Cox, B. G. *Acids and Bases Solvent Effects on Acid−Base Strength*; Oxford University Press: Oxford, 2013.

(4) (a) Emond, M.; Sun, J.; Grégoire, J.; Maurin, S.; Tribet, C.; Jullien, L. *Phys. Chem. Chem. Phys.* **2011**, *13*, 6493−6499. (b) Emond, M.; Le Saux, T.; Allemand, J.-F.; Pelupessy, P.; Plasson, R.; Jullien, L. *Chem. - Eur. J.* **2012**, *18*, 14375−14383.

(5) (a) Ito, H. *Adv. Polym. Sci.* **2005**, *172*, 37. (b) Shirai, M.; Tsunooka, M. *Bull. Chem. Soc. Jpn.* **1998**, *71*, 2483.

(6) Menard, E.; Meitl, M. A.; Sun, Y.; Park, J.-U.; Shir, D. J.-L.; Nam, Y.-S.; Jeon, S.; Rogers, J. A. *Chem. Rev.* **2007**, *107*, 1117.

(7) Serafinowski, P. J.; Garland, P. B. *J. Am. Chem. Soc.* **2003**, *125*, 962.

(8) Geißler, D.; Antonenko, Y. N.; Schmidt, R.; Keller, S.; Krylova, O. O.; Wiesner, B.; Bendig, J.; Pohl, P.; Hagen, V. *Angew. Chem.* **2005**, *117*, 1219.

(9) Yue, X. L.; Yanez, C. O.; Yao, S.; Belfield, K. D. *J. Am. Chem. Soc.* **2013**, *135*, 2112.

(10) (a) Simkovitch, R.; Shomer, S.; Gepshtein, R.; Huppert, D. *J. Phys. Chem. B* **2015**, *119*, 2253. (b) Agmon, N. *J. Phys. Chem. A* **2005**, *109*, 13. (c) Tolbert, L. M.; Solntsev, K. M. *Acc. Chem. Res.* **2002**, *35*, 19. (d) Ireland, J. F.; Wyatt, P. A. *Adv. Phys. Org. Chem.* **1976**, *12*, 131.

(11) (a) Szczepanik, B. *J. Mol. Struct.* **2015**, *1099*, 209. (b) Mohammed, O. F.; Pines, D.; Nibbering, E. T. J.; Pines, E. *Angew. Chem.* **2007**, *119*, 1480.

DOI: 10.1021/acs.joc.6b01991
J. Org. Chem. 2016, 81, 10942−10954

(12) See for example: (a) Solntsev, K. M.; Clower, C. E.; Tolbert, L. M.; Huppert, D. *J. Am. Chem. Soc.* **2005**, *127*, 8534. (b) Poizat, O.; Bardez, E.; Buntinx, G.; Alain, V. *J. Phys. Chem. A* **2004**, *108*, 1873. (c) Kim, T. G.; Kim, Y.; Jang, D.-J. *J. Phys. Chem. A* **2001**, *105*, 4328. (d) Bardez, E.; Chatelain, A.; Larrey, B.; Valeur, B. *J. Phys. Chem.* **1994**, *98*, 2357.
(13) Pérez-Lustres, J. L.; Rodriguez-Prieto, F.; Mosquera, M.; Senyushkina, T. A.; Ernsting, N. P.; Kovalenko, A. *J. Am. Chem. Soc.* **2007**, *129*, 5408.
(14) Ihmels, H.; Schäfer, K. *Photochem. Photobiol. Sci.* **2009**, *8*, 309.
(15) Granzhan, A.; Ihmels, H.; Tian, M. *Arkivoc* **2015**, *vi*, 494.
(16) Bradsher, C. K. *Chem. Rev.* **1946**, *38*, 447.
(17) (a) Earley, W. G.; Kumar, V.; Mallamo, J. P.; Subramanyam, C.; Dority, J. A., Jr.; Miller, M. S.; DeHaven-Hudkins, D. L.; Aimone, L. D.; Kelly, M. D.; Ault, B. *J. Med. Chem.* **1995**, *38*, 3586. (b) Earley, W. G.; Dority, J. A., Jr.; Kumar, V.; Malamo, J. P. *Heterocycles* **1995**, *41*, 309. (c) Bradsher, C. K.; Yarrington, N. *J. Org. Chem.* **1960**, *25*, 294. (d) Bradsher, C. K.; Jones, J. H. *J. Am. Chem. Soc.* **1957**, *79*, 6033.
(18) Britton, H. T. S.; Robinson, R. A. *J. Chem. Soc.* **1931**, 458.
(19) Polster, J.; Lachmann, H. *Spectrometric Titrations: Analysis of Chemical Equilibria*; VCH: Weinheim, 1989.
(20) Weller, A. *Z. Elektrochem.* **1952**, *56*, 662.
(21) Le Bahers, T.; Adamo, C.; Ciofini, I. *J. Chem. Theory Comput.* **2011**, *7*, 2498.
(22) Cimino, P.; Raucci, U.; Donati, G.; Chiariello, M. G.; Schiazza, M.; Coppola, F.; Rega, N. *Theor. Chem. Acc.* **2016**, *135*, 117.
(23) (a) Yates, K.; Wai, H. *J. Am. Chem. Soc.* **1964**, *86*, 5408. (b) Christodouleas, N.; Hamill, W. H. *J. Am. Chem. Soc.* **1964**, *86*, 5413.
(24) Hansch, C.; Leo, A.; Taft, R. W. *Chem. Rev.* **1991**, *91*, 165.
(25) (a) Faulhaber, K.; Granzhan, A.; Ihmels, H.; Otto, D.; Thomas, L.; Wells, S. *Photochem. Photobiol. Sci.* **2011**, *10*, 1535. (b) Ihmels, H.; Faulhaber, K.; Engels, B.; Lennartz, C. *Chem. - Eur. J.* **2000**, *6*, 2854.
(26) Tolbert, L. M.; Haubrich, J. E. *J. Am. Chem. Soc.* **1994**, *116*, 10593.
(27) (a) Finkler, B.; Spies, C.; Vester, M.; Walte, F.; Omlor, K.; Riemann, I.; Zimmer, M.; Stracke, F.; Gerhards, M.; Jung, G. *Photochem. Photobiol. Sci.* **2014**, *13*, 548. (b) Agmon, N.; Huppert, D.; Masad, A.; Pines, E. *J. Phys. Chem.* **1991**, *95*, 10407.
(28) (a) Malval, J.-P.; Chaumeil, H.; Rettig, W.; Kharlanov, V.; Diemer, V.; Ay, E.; Morlet-Savary, F.; Poizat, O. *Phys. Chem. Chem. Phys.* **2012**, *14*, 562. (b) Malval, J.-P.; Diemer, V.; Morlet Savary, F.; Jacques, P.; Allonas, X.; Chaumeil, H.; Defoin, A.; Carré, C. *Chem. Phys. Lett.* **2008**, *455*, 238.
(29) (a) Simkovitch, R.; Karton-Lifshin, N.; Shomer, S.; Shabat, D.; Huppert, D. *J. Phys. Chem. A* **2013**, *117*, 3405. (b) Karton-Lifshin, N.; Albertazzi, L.; Bendikov, M.; Baran, P. S.; Shabat, D. *J. Am. Chem. Soc.* **2012**, *134*, 20412.
(30) (a) Suppan, P.; Ghoneim, N. *Solvatochromism*; RSC: London, 1997. (b) Reichardt, C. *Solvents and Solvent Effects on Organic Chemistry*, 3rd ed., Wiley-VCH: Weinheim, 2003, Chapter 4.2.
(31) (a) Kulinich, A. V.; Ishchenko, A. A. *Russ. Chem. Rev.* **2009**, *78*, 141. (b) Cavalli, V.; da Silva, D. C.; Machado, C.; Machado, V. G.; Soldi, V. *J. Fluoresc.* **2006**, *16*, 77.
(32) Pruka, D.; Prukala, W.; Gierszewski, M.; Karolczak, J.; Khmelinskii, I.; Sikorski, M. *Dyes Pigm.* **2014**, *108*, 126.
(33) (a) Chen, K.; Shu, Q.; Schmittel, M. *Chem. Soc. Rev.* **2015**, *44*, 136. (b) Daly, B.; Ling, J.; de Silva, A. P. *Chem. Soc. Rev.* **2015**, *44*, 4203. (c) Yang, Z.; Cao, J.; He, Y.; Yang, J. H.; Kim, T.; Peng, X.; Kim, J. S. *Chem. Soc. Rev.* **2014**, *43*, 4563. (d) You, Y.; Nam, W. *Chem. Sci.* **2014**, *5*, 4123. (e) Yao, J.; Yang, M.; Duan, Y. *Chem. Rev.* **2014**, *114*, 6130. (f) Carter, K. P.; Young, A. M.; Palmer, A. E. *Chem. Rev.* **2014**, *114*, 4564. (g) Pal, S.; Chatterjee, N.; Bharadwaj, P. K. *RSC Adv.* **2014**, *4*, 26585. (h) Panchenko, P. A.; Fedorova, O. A.; Fedorov, Y. V. *Russ. Chem. Rev.* **2014**, *83*, 155. (i) Li, X.; Gao, X.; Shi, W.; Ma, H. *Chem. Rev.* **2014**, *114*, 590.
(34) Bortolozzi, R.; von Gradowski, S.; Ihmels, H.; Schäfer, K.; Viola, G. *Chem. Commun.* **2014**, *50*, 8242.
(35) Tang, Y.; Wei, J.; Zhong, W.; Liu, W. X. M. *Heteroat. Chem.* **2010**, *21*, 423.
(36) Bradsher, C. K.; Parham, J. C. *J. Org. Chem.* **1963**, *28*, 83.
(37) Jones, G.; Jackson, W. R.; Choi, C. Y.; Bergmark, W. R. *J. Phys. Chem.* **1985**, *89*, 294−300.

DOI: 10.1021/acs.joc.6b01991
J. Org. Chem. 2016, 81, 10942−10954